REFERENCES AND NOTES

1. W. Goodman, *Science*, in press.
2. G. Pirug, G. Broden, H. P. Bonzel, in *Proceedings of the Seventh International Vacuum Congress and the Third International Conference on Solid Surfaces*, R. Dobrozemsky, F. Rüdenauer, F. P. Viehböck, A. Breth, Eds. (R. Dobrozemsky *et al.*, Vienna, 1977), p. 907.
3. J. Estermann and O. Stern, *Z. Phys.* **61**, 95 (1930).
4. D. V. Tendulkar and R. E. Stickney, *Surf. Sci.* **27**, 516 (1971).
5. M. J. Cardillo and G. E. Becker, *Phys. Rev. Lett.* **42**, 508 (1979).
6. K. H. Rieder and T. Engel, *ibid.* **43**, 373 (1979).
7. M. Manninen *et al.*, *Phys. Rev. B* **29**, 2314 (1984).
8. V. Celli, D. Eichenauer, A. Kaufhold, J. P. Toennies, *ibid.* **32**, 5044 (1985).
9. D. S. Kaufman, R. M. Aten, E. H. Conrad, L. R. Allen, T. Engel, in preparation.
10. D. Haneman and R. Haydock, *J. Vac. Sci. Technol.* **21**, 330 (1982).
11. D. R. Hamann, *Phys. Rev. Lett.* **46**, 1227 (1981).
12. J. Tersoff, M. J. Cardillo, D. R. Hamann, *Phys. Rev. B* **32**, 5044 (1985).
13. M. J. Cardillo *et al.*, *ibid.* **28**, 494 (1983).
14. K. Kern, R. David, R. L. Palmer, G. Comsa, *Phys. Rev. Lett.* **56**, 620 (1986).
15. L. J. Gomez, S. Bourgeal, J. Ibanez, M. Salmeron, *Phys. Rev. B* **31**, 2551 (1985).
16. E. H. Conrad *et al.*, *J. Chem. Phys.* **84**, 1015 (1986). See also an erratum to this paper (*ibid.*, in press).
17. B. Poelsma, L. K. Verheij, G. Comsa, *Phys. Rev. Lett.* **53**, 2500 (1984).
18. ———, *ibid.* **49**, 1731 (1982).
19. J. P. Toennies and K. Winkelmann, *J. Chem. Phys.* **66**, 3965 (1977).
20. T. Engel, D. Braid, E. H. Conrad, *Rev. Sci. Instrum.* **57**, 487 (1986).
21. M. P. D'Evelyn and R. J. Madix, *Surf. Sci. Rep.* **3**, 413 (1983).
22. T. Engel and K. H. Rieder, *Springer Tracts in Modern Physics* (Springer-Verlag, Berlin, 1982), vol. 91.
23. K. H. Rieder, *Contemp. Phys.* **26**, 559 (1985).
24. J. A. Barker and D. J. Auerbach, *Surf. Sci. Rep.* **4**, 1 (1984).
25. T. Engel and K. H. Rieder, *Surf. Sci.* **109**, 140 (1981).
26. B. Poelsma and G. Comsa, *Faraday Discuss. Chem. Soc.* **80** (no. 16) 1 (1985).
27. E. H. Conrad, L. R. Allen, D. Blanchard, T. Engel, in preparation.
28. J. P. Toennies, *Appl. Phys.* **3**, 91 (1974).
29. B. Poelsma, L. K. Verheij, G. Comsa, *Phys. Rev. Lett.* **51**, 2410 (1983).
30. K. D. Gibson and S. J. Sibener, *ibid.* **55**, 1514 (1985).

Polarized Electron Probes of Magnetic Surfaces

ROBERT J. CELOTTA AND DANIEL T. PIERCE

The magnetic properties of surfaces are now being explored with electron spectroscopies that use electron spin polarization techniques. The increased activity in surface magnetic measurements with polarized electron beams is spurred by new scientific and technological challenges and is made feasible by recent advances in the technology of sources and detectors of polarized electrons. The ability to grow thin films and to engineer artificial structures permits new phenomena to be investigated at magnetic surfaces and interfaces. For such investigations, spin-polarized electron techniques—such as polarized electron scattering, polarized photoemission, polarized Auger spectroscopy, and scanning electron microscopy with polarization analysis—have been and will probably continue to be used to great advantage.

MUCH OF WHAT WE KNOW ABOUT SURFACES ON THE atomic level comes from electron-based measurements. Our knowledge of microstructures in general is largely a consequence of rapid advancement in the field of electron microscopy. It is therefore surprising that use has not been made of the full information content of an electron beam, in particular the degree of electron spin polarization.

Electron-based measurements typically determine the change in momentum of an incident probing electron, the momentum distribution of emitted electrons, or, in the case of the scanning electron microscope, simply the number of emitted electrons. Since 1925, however, it has been known (*1*) that each electron possesses a spin, with an associated magnetic dipole moment having a fixed strength and variable orientation in space. It is this additional degree of freedom, the orientation of the electron spin, that is the key to obtaining more information about the system under study.

A fully characterized electron beam has either been prepared with or measured to have a specific momentum and polarization. The polarization of an electron beam in the z direction is defined as

$$P_z = \frac{N_\uparrow - N_\downarrow}{N_\uparrow + N_\downarrow} \quad (1)$$

where $N_\uparrow$ (or $N_\downarrow$) represents the number of electron spins parallel (or antiparallel) to the z direction. A completely polarized electron beam has a polarization vector magnitude of unity, compared to an "ordinary" beam with a polarization of zero.

Macroscopic fields, such as those used to separate atoms of differing spins in a Stern-Gerlach experiment, cannot be used (*2*) with free electrons to filter out those electrons with a particular spin direction to form a highly polarized beam. While many clever ways (*2*) of producing and detecting electron polarization have been suggested during the last 50 years, only recently have polarized electron sources and detectors progressed to the stage where they may be used routinely in experiments. This accounts in large measure for the relative paucity of experimental results in the field.

Measurement of the polarization of an electron beam makes it possible to learn more about systems in which interactions affecting the spin of the electron occur. The spin-orbit and exchange interactions do this in fundamentally different ways. In the spin-orbit interaction, the magnetic dipole of the incident electron interacts with the electric field of an atom in the sample. This is a relativistic effect that is largest for heavy atoms and can cause a redistribution of the direction of the spins, that is, a change in the polarization. The exchange interaction comes about as a consequence of the Pauli exclusion principle, which forbids any two electrons from having exactly the same quantum numbers. Hence, the spatial part of the wave function of two colliding electrons with the same spin direction will be different from that of two electrons with opposite

The authors are in the Radiation Physics Division at the National Bureau of Standards, Gaithersburg, MD 20899.

spin directions. The result is that the cross section or probability of such a scattering event depends on the relative orientation of the two spins. In this way a polarized electron beam can detect the orientation of target spins through measurement of the scattering probability as a function of the incident electron polarization direction. The surface region is probed by the electrons because of the short electron mean free paths, of order 1 nm at the energies used in surface spectroscopies. Thus the Pauli exclusion principle is responsible for the magnetic sensitivity of the method, and the strong electron-solid interaction is responsible for its surface sensitivity. The strongly interacting polarized electrons can be used to answer questions about surface magnetism in much the same way that weakly interacting neutrons have been used to study magnetism in the bulk.

This article briefly describes recent advances in the technology of producing and detecting spin-polarized electron beams and presents four illustrations of surface magnetic phenomena studied with new, spin-polarized electron spectroscopies. A view of the scientific and technological challenges that can be addressed by taking advantage of the information in electron spin polarization measurements concludes the discussion.

Polarized Electron Sources and Detectors

The development of a source (*3*) of spin-polarized electrons based on circularly polarized light–induced photoemission from GaAs (*4*) represented a turning point in the use of polarized electron beams. Before this development, polarized beams were generally of low intensity, with currents orders of magnitude less than those that could be obtained with a conventional electron gun. In the GaAs spin-polarized electron gun, a GaAlAs diode laser is typically used to illuminate a GaAs surface treated with cesium and oxygen to produce a highly efficient, negative–electron affinity photoemitter. The angular momentum of the circularly polarized incident light is effectively transferred to the emerging electron beam during the photoemission process. A reversal of the sense of the circular polarization of the light reverses the polarization of the electron beam without affecting its intensity, so that experiments in which the electron spin direction is modulated may be easily performed. In such an experiment, any modulation of the signal observed after a scattering event indicates the magnitude of a spin-dependent scattering effect. Beam polarizations approaching 50% have been achieved with beam currents equivalent to those in conventional electron guns (tens of microamperes in low-energy operation).

Spin polarization analyzers have not yet reached the near-unity efficiency that electron multipliers display when used as particle counters. Most spin detectors are based on scattering of the electron beam to be analyzed from a high atomic number target, so that the spin-orbit effect can transform a net polarization into an asymmetry in the spatial distribution of the scattered particles. Measurement of the spatial asymmetry with multiple detectors allows the electron spin polarization to be determined. The first such devices, known as Mott detectors (*2*), were developed to study the polarization of electrons in β decay. Mott detectors usually operate at scattering energies near 100 keV. At these energies, most of the electrons penetrate the thin gold foils used as scattering targets, and typically only about 10^{-4} of the incident beam is collected in the measurement of the asymmetry.

Recently, low-energy spin analyzers (*5*, *6*) have been developed that are as efficient as optimized high-energy detectors. The low energy required for operation makes them more compact and easier to use. The newest polarization analyzer (*6*) relies on low-energy (150 eV) diffuse backscattering from thick polycrystalline gold films followed by channel plate electron multiplier detection. (An application of this analyzer to obtain high-resolution images of magnetic microstructure is described below.)

Temperature Dependence of Spin Ordering: Polarized Electron Scattering

The long-range order of electron spins characteristic of a ferromagnet can be investigated, for example, by spin-polarized electron scattering. The change in the ordering of the spins, and hence in the magnetization as a function of temperature, is a salient feature of a magnetic system. As the temperature is increased from 0 K, the excitation of spin waves, or magnons, causes the spins to deviate from their previously perfect alignment. At the high end of the temperature range, the Curie temperature (T_c) marks the critical point where the ferromagnet undergoes a second-order phase transition to the paramagnetic phase, in which there is no long-range magnetic order. Near this critical temperature, spin fluctuations dominate the physical behavior. Striking analogs of this phase transition can be found in such diverse systems as liquids, superconductors, ferroelectrics, and liquid crystals, thereby revealing the exciting universal nature of critical phenomena.

Spin-polarized electron scattering is especially suited to the study of magnetization near the surface. The interaction of an electron beam with a magnetic surface is governed by the Hamiltonian

$$\mathcal{H} = V + V_{so} + \sum_j J(\vec{r} - \vec{R}_j)\vec{s} \cdot \vec{S}_j \qquad (2)$$

where V is the spin-independent part of the scattering and V_{so} is the spin-dependent part due to the spin-orbit interaction, the effect of which can be isolated experimentally. The last term is the spin-dependent exchange interaction between the incident electron spin

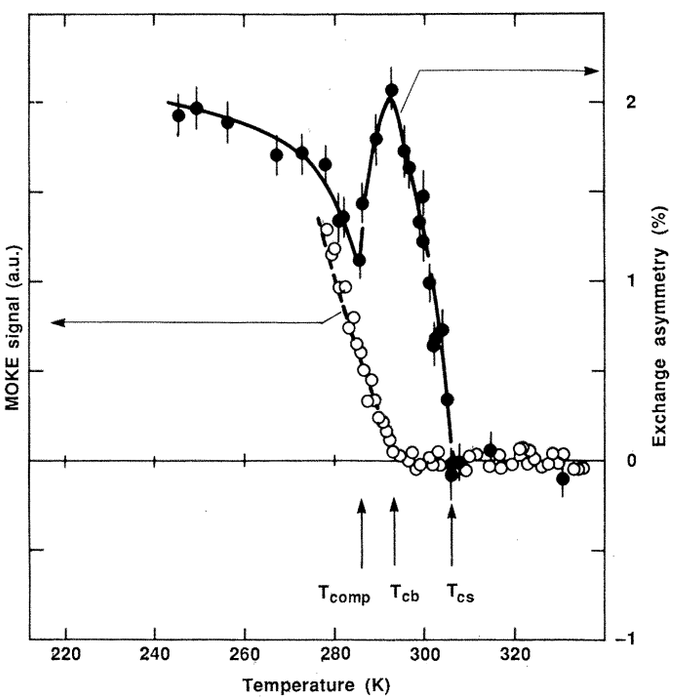

Fig. 1. The temperature dependence of the asymmetry (●) in the scattering of 62.6-eV polarized electrons from a 50-nm-thick Gd(0001) film compared to the temperature dependence of the bulk magnetization (○) measured by MOKE. The surface magnetization exhibits a critical transition at T_{cs} = 307 K, in contrast to the bulk transition at T_{cb} = 293 K. [From (*14*)]

$\vec{s}$ at position $\vec{r}$ and the spin of the atom $\vec{S}_j$ at position $\vec{R}_j$, with $J(\vec{r} - \vec{R}_j)$ giving the strength of the exchange coupling. The scattering is sensitive to the size of the atomic magnetic moments, which are proportional to $\vec{S}_j$, as well as their orientation and degree of order. Experimentally the intensity asymmetry A is measured in the elastic scattering of a spin-polarized electron beam from a ferromagnetic surface, where A is defined as

$$\frac{1}{P}\frac{I_{\uparrow\uparrow} - I_{\uparrow\downarrow}}{I_{\uparrow\uparrow} + I_{\uparrow\downarrow}} \tag{3}$$

In Eq. 3, $I_{\uparrow\uparrow}$ is the scattered intensity when the magnetic moment of the incident electron is parallel to the magnetization, and $I_{\uparrow\downarrow}$ is the intensity when it is antiparallel. The factor $1/P$ takes into account the fact that the incident-beam polarization P may be less than unity. The greater the alignment of the spins in the ferromagnet, the greater the scattering asymmetry for a particular material. For single scattering, A is directly proportional to $M_s(T)$, where M_s is the magnetization of the surface region probed by the electron beam at some temperature T. This proportionality will not hold in general because of multiple scattering (*7*), but it is a good approximation for backscattering from an amorphous ferromagnet (*8*) or in scattering from a ferromagnetic crystal near T_c (*9*).

Spin-dependent electron scattering from an amorphous ferromagnet or ferromagnetic glass has been used to determine the temperature dependence of the magnetization at low temperature (*8*). For the bulk, the relative magnetization at low temperature follows the Bloch $T^{3/2}$ law

$$M(T)/M(0) = 1 - BT^{3/2} + \ldots \tag{4}$$

Because of the different boundary conditions at the surface—essentially the lack of translational periodicity—Rado (*10*) and Mills and Maradudin (*11*) predicted that the temperature dependence of the surface magnetization would be the same as that of the bulk but that the coefficient B for the surface would be twice that of the bulk. Measurement of the asymmetry (*8*) in the spin dependence of electron scattering from the ferromagnetic glass confirmed the prediction that the relative surface magnetization obeys the $T^{3/2}$ power law but found a coefficient B three times that for the bulk. This larger than predicted increase in B suggests that there is a further effect not accounted for in the theory, such as a smaller exchange coupling between surface and bulk atoms than between bulk atoms alone.

At the other end of the temperature range where ferromagnetism exists, that is, near the critical temperature, the behavior of the magnetization at the surface of a ferromagnet may be different than the behavior of the bulk, but it is nevertheless influenced by the properties of the bulk. If the exchange coupling J_s between surface spins is the same as the exchange coupling J_b of the bulk spins, then the surface and bulk spins become ordered at the same temperature. If the coupling in the surface is enhanced beyond a certain critical value, however, a pure surface transition becomes possible in which the surface magnetization undergoes a critical ordering transition at a temperature greater than the bulk Curie temperature (T_{cb}), that is, ordered surface spins exist on top of disordered bulk spins (*12*). The former case of identical surface and bulk critical temperatures has been observed on the (100) and (110) surfaces of a nickel single crystal (*13*) and the latter case of surface-enhanced magnetic order has been observed on the (0001) surface of an expitaxially grown gadolinium film (*14*). Spin-polarized electron scattering was used in each case to make the first experimental study of each type of transition.

To gain some idea of how different the temperature dependence of the surface magnetization is from that of the bulk, note that the bulk magnetization generally follows a Brillouin function, whereas the surface magnetization is expected to exhibit a linear temperature dependence over a wide temperature range. Near the critical temperature, the temperature dependence of the surface and bulk magnetization has the same functional form, which for the surface is written as

$$M_s(T) \propto (1 - T/T_{cs})^{\beta_1} \tag{5}$$

where T_{cs} is the surface Curie temperature and β_1 is the critical exponent for long-range order in the first layer. Alvarado and colleagues (*13*) measured the asymmetry in the scattering of spin-polarized electrons from the (100) and (110) faces of nickel and determined β_1 to be 0.81 ± 0.02 and 0.79 ± 0.02, respectively. Recently, a value of $\beta_1 = 0.78 \pm 0.02$ has been found from Monte Carlo calculations for a three-dimensional Ising model (*15*) and a value of $\beta_1 = 0.84 \pm 0.02$ has been calculated using a renormalization group approach for the Heisenberg model (*16*). The experimental and theoretical uncertainties are still too large to allow an unequivocal distinction between the Ising and Heisenberg universality classes. Note that the value of β_1 for the surface of a semi-infinite ferromagnet is different from the value of β ($\simeq 1/3$) for the bulk.

Surface-enhanced magnetic order is exhibited in the case of the (0001) surface of the rare earth gadolinium, where T_{cs} is higher than T_{cb}. This can be seen in Fig. 1, which compares the measured asymmetry in spin-dependent elastic scattering with the relative magnetization as measured with the magneto-optic Kerr effect (MOKE). Since this optical measurement samples the outer 15 to 20 nm of the material, it is considered to represent the temperature dependence of the bulk magnetization. The amount by which T_{cs} increases relative to T_{cb} depends somewhat on the details of the gadolinium film preparation. In particular, T_{cs} is sensitive to surface contamination. For intentionally contaminated films, T_{cs} is equal to T_{cb}, as observed for nickel.

The peculiar minimum observed at 289 K, labeled T_{comp} in Fig. 1, can be explained by a different effect: the exchange coupling between the surface layer and the bulk is such that the surface is predominantly antiferromagnetically coupled to the bulk. The minimum at T_{comp} occurs when the contribution to the scattering asymmetry from the bulk becomes less with increasing temperature than the contribution from the surface. Between T_{comp} and T_{cb}, the scattering asymmetry increases as the surface magnetization becomes less determined by the decreasing bulk magnetization and rotates into the direction of the magnetizing field. Spin-resolved photoemission measurements (*14*) at temperatures below T_{comp} confirm this picture of an antiferromagnetically coupled surface layer.

Electronic Structure and Magnetism: Polarized Photoemission

The electronic structure—that is, the energy and momentum states for electrons in a solid—is what determines the solid's cohesive energy and its optical, electronic, and magnetic properties. The band structure, which describes the dispersion of electron energy $E(\vec{k})$ with momentum $\vec{k}$, has been investigated by energy- and angle-resolved photoemission spectroscopy. Information about the initial-state energy and momentum can be obtained by measuring the energy and angle (momentum) of the emitted electrons. The photoelectron's kinetic energy E_K is related to the initial- and final-state energy $E_i(\vec{k}_i)$ and $E_f(\vec{k}_f)$ by

$$E_K = E_f(\vec{k}_f) - E_v = E_i(\vec{k}_i) + \hbar\omega - E_v \tag{6}$$

where E_v is the vacuum energy and $\hbar\omega$ is the photon energy. There is a complementary technique known as inverse photoemission (or bremsstrahlung isochromat) spectroscopy, which probes the unfilled states and in particular can give information about unfilled states between the Fermi energy and E_v (which are otherwise inaccessible to photoemission). In this case the kinetic energy is that of the incoming electron at an energy $E_i(\vec{k}_i)$ which scatters inelastically to the final state $E_f(\vec{k}_f)$, emitting a photon $\hbar\omega$, as described by

$$E_K = E_i(\vec{k}_i) - E_v = E_f(\vec{k}_f) + \hbar\omega - E_v \quad (7)$$

which is analogous to Eq. 6.

In a ferromagnet, the band structure also depends on the electron spin. Electrons with magnetic moments parallel to the magnetization have a lower energy than those with opposite orientation. Such exchange-split energy bands are of special interest in the case of the incompletely filled *d* shells of transition metal ferromagnets. The spin-dependent electronic structure can be investigated explicitly by measuring the energy, angle, and spin polarization of photoemitted electrons. Similarly, in inverse photoemission the electronic structure can be investigated by observing the dependence of the emitted photon intensity on the energy, angle, and spin polarization of the incident electron beam. Thus the spin of electronic states can be measured in both photoemission and inverse photoemission by adding a spin analyzer or a spin-polarized electron gun, respectively.

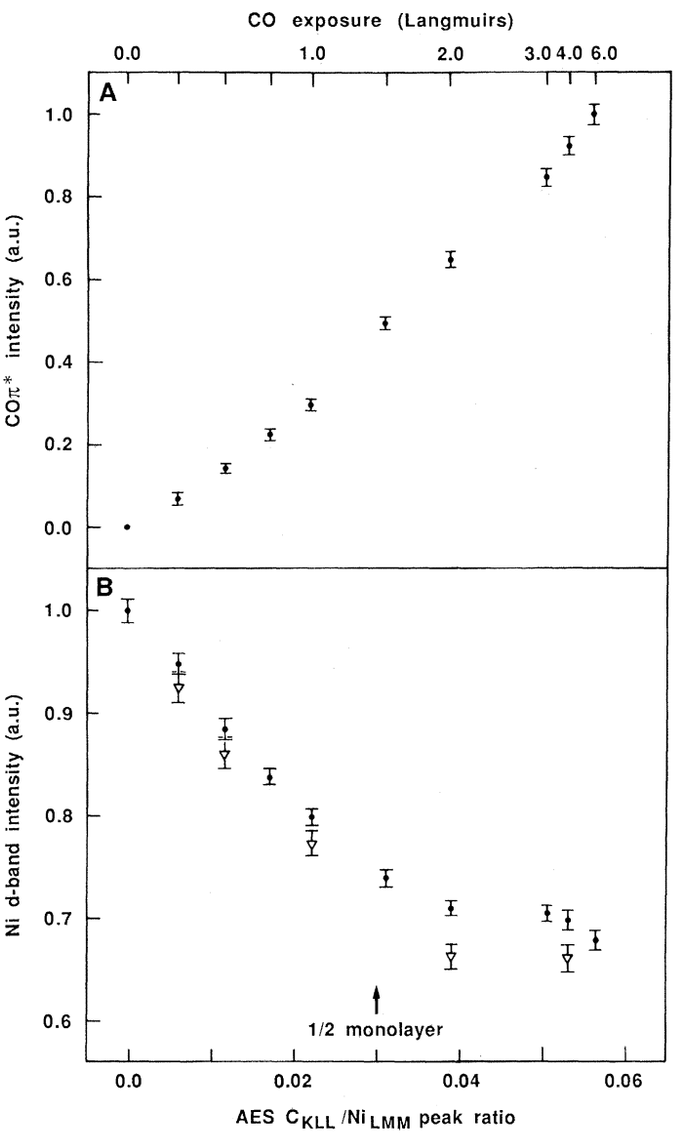

Fig. 2. The intensity of peaks in the inverse photoemission spectrum of Ni(110) as a function of CO coverage in terms of the AES peak ratio of carbon (272 eV) to nickel (848 eV). The intensity of the peak originating from transitions into the CO π^* level (A) increases continuously over the range pictured. (B) The minority-spin *d*-band final state. Symbols: (●) spin-integrated data; (▽) minority-spin data. [From (*20*)]

An important success of spin-polarized photoemission was the investigation (*17*) of the electronic structure of iron and its relation to ferromagnetism at nonzero temperatures. It is generally agreed that for iron the simple Stoner model, in which the magnetic moment decreases to 0 at T_c, does not apply; instead, local magnetic moments at each atom site persist beyond T_c. The loss of spontaneous magnetization then depends on thermal disorder of local moments. The current question centers on the degree of short-range magnetic order, that is, on the spatial extent of the magnetic correlations between neighboring magnetic moments. Spin-resolved photoemission measurements (*17*) of Fe(100) show exchange-split peaks originating from states near the Γ point at the center of the Brillouin zone. The splitting is unchanged at temperatures from 0.3 T_c to 0.85 T_c, but there are changes in peak intensities. For example, the prominent peak in the minority-spin spectrum decreases with increasing temperature, and intensity increases at an energy corresponding to the peak in the majority-spin spectrum. This consequence of increased spin density fluctuations with temperature can be observed with spin-resolved (but not spin-integrated) photoemission measurements. In the absence of well-defined surface states, the photoemission spectra reflect the bulk electronic structure and have been discussed in terms of the theories of finite temperature magnetism that so far exist only for the bulk. To estimate the extent of the short-range order, Haines and colleagues (*18*) calculated spin-resolved photoemission spectra for iron clusters with various degrees of assumed magnetic order. Their calculations bridged the gap between the "disordered local-moment picture," in which there is no short-range order of the magnetic moments, and the "local band picture," in which there is significant short-range order and a magnetically correlated region large enough to define ferromagnetic bands. From a comparison with the experimental results, they concluded that iron has short-range magnetic order of at least 0.4 nm near T_c.

Another study of the relation between surface electronic structure and magnetism is that of the change induced by the chemisorption of CO on the Ni(110) surface. The spin-up (majority) *d* states in nickel are occupied, but there is approximately one-half of a spin-down (minority) hole or unoccupied *d* state per nickel atom. A key ingredient to ferromagnetism in nickel, these minority-spin *d* holes lie in a flat band just above the Fermi level (E_F). In a spin-polarized inverse photoemission spectrum of nickel, there is a large peak in the photon intensity at an energy just above E_F only in the minority-spin spectrum, reflecting the high probability for minority-spin incident electrons to make transitions into the *d*-hole states (*19*).

The relation between magnetism and chemisorption has traditionally been explored by using bulk magnetic measurements and high surface area samples. In fact, bulk magnetic measurements of dispersed catalysts have been used to monitor chemical reactions. Neither the bulk measurements nor the limited surface magnetic measurements could determine whether the chemisorption-induced reduction in surface magnetism was due to a disruption of the long-range ordering of the magnetic moments or to a reduction of the magnetic moments themselves. If the reduction in surface magnetization was due to the loss of long-range order, a decrease in the minority-spin inverse photoemission peak with a concomitant growth of a peak in the spectrum for the opposite spin orientation would be expected; this is because, in the absence of long-range

order, there is an equal number of up- and down-spin states. What was observed for the chemisorption of CO on Ni(110) (*20*) was a reduction in the intensity of the minority-spin peak without any significant change in the majority-spin intensity. This led to the conclusion that the CO reduces the surface magnetism by reducing the magnetic moment (or net spin) of the nickel atoms.

More can be learned about the reduction of the surface magnetism from Fig. 2. The peak at 3.7 eV above E_F (Fig. 2A) is due to transitions into the π^* antibonding level of CO. This peak continues to increase with increasing CO coverage, indicating a continued adsorption of CO. From spin-resolved measurements it was determined that the major contribution to and changes in the spin-integrated nickel *d* peak intensity originate in the minority-spin intensity. Therefore, plotted along with the minority-spin intensity in Fig. 2B is the spin-integrated *d*-band intensity, which is more easily measured. The *d*-band intensity decreases up to a coverage of one-half monolayer [Auger electron spectrosopy (AES) peak ratio, 0.03] and then is constant. From the amount of peak reduction and its saturation at one-half monolayer coverage, it was concluded that the adsorption of one CO molecule eliminates the equivalent of two nickel surface atom magnetic moments (*20*).

Element-Specific Local Magnetization: Polarized Auger Spectroscopy

One of the most widely used surface analysis techniques, AES is not only surface-sensitive, but the Auger electron energies are characteristic of the element from which the electrons are emitted. This elemental specificity is the basis for the use of AES in surface science to detect minute quantities of a substance, frequently a contaminant, on a surface. If done with care, AES provides a reasonably quantitative compositional analysis of the surface. Careful analysis of small shifts in Auger energies or changes in peak shapes can also provide information about the details of the electronic structure of the emitting atom and its surroundings.

In the case of a ferromagnet, the emitted Auger electrons may be spin-polarized. The origin of the spin polarization varies for different elements or for different transitions of the same element. It has been found that information can be obtained about the local magnetization at the site of a particular element when valence states are involved in the Auger decay (*21*). When only core levels are involved in the Auger decay, there is still a spin polarization that arises from the interaction of the net spin density of the magnetic valence electrons with the partly filled core levels. Although spin-polarized AES is a recently developed technique, it can be used for studies of surface magnetism and as a means to gain information about the intricacies of the Auger process itself.

As an example, consider the Auger transition in iron labeled as $M_{23}\ M_{45}\ M_{45}$. In this transition, an incident electron or x-ray photon excites an electron from the iron 3*p* shell. A valence electron then falls into the empty 3*p* core state, giving up the precise amount of energy by which the two states are separated. Another valence electron is emitted with this kinetic energy, thus conserving overall energy. (In this discussion we ignore details such as screening of the holes by other electrons.) The process can be written as

$$3p^6 3d^n + \hbar\omega \rightarrow 3p^5 3d^n + e \rightarrow 3p^6 3d^{n-2} + e_{\text{Auger}} + e$$

The intensity and polarization of this Auger line centered at 43 eV are determined by the two *d* holes and are well reproduced by a self-convolution of the spin-split valence density of states (*21*). There is a significant spin polarization of this intense Auger line ($P = 37\%$). The sign is positive because most of the *d* electrons have magnetic moments parallel to the magnetization.

In gadolinium, there is again a transition suitable for monitoring the local magnetization: the $N_{45}\ N_{67}\ N_{67}$ Auger line at 133 eV, wherein a 4*d* hole is created and filled by an electron from the half-filled 4*f* shell ($^8S_{7/2}$ spin configuration with all seven spins parallel) and another 4*f* electron is emitted (*22*). The magnetic moment of this Auger electron is parallel to the magnetization in gadolinium. Thus in both iron and gadolinium there are suitable transitions that allow the sign and magnitude of the local magnetization to be monitored.

Spin-polarized AES is powerful because of its ability to determine the local magnetization. Important qualitative conclusions can be reached without detailed analysis, as revealed in the example of a monolayer of gadolinium evaporated on an Fe(100) surface (*22*) (Fig. 3). Here the polarization of the gadolinium is opposite that of the iron; that is, the monolayer of gadolinium is magnetically ordered and couples antiferromagnetically to the Fe(100) substrate. Even in the initial stages of the deposition of gadolinium, corresponding to an average film thickness of 0.1 monolayer, the effective polarization of the gadolinium Auger lines remains unchanged. This suggests that even isolated gadolinium atoms align their moments opposite to the iron magnetization. Although antiparallel coupling between rare earths and transition metals has been observed in a number of crystalline and amorphous alloys, it is clear from this study that no special three-dimensional rare earth–transition metal coordination or rare earth–rare earth coupling is necessary.

The interface between gadolinium and iron was further investigated by measuring the temperature dependence of the magnetization of each element individually. The iron polarization signal, which is primarily from the interface layer, decreased approximately linearly toward an extrapolated value of T_c less than the bulk value. This suggests that the gadolinium weakens the magnetic coupling of the outermost layer of iron to the bulk. Clearly, spin-polarized AES is a useful way to investigate the magnetic properties of a surface or even to "look through" a film of a few layers to the interface.

Magnetic Microstructure: Scanning Electron Microscopy with Polarization Analysis

There are many scientifically interesting and technologically important questions about magnetic microstructure that need to be answered. Although one can list the multiple terms that should be included in the Hamiltonian for the system to give rise to microscopic ferromagnetic domains, it is not yet possible to calculate which of the many possibilities will result. The structure of domain walls is of interest, as well as the influence of size effects, dimensionality (for example, the presence of a surface), impurities, and various anisotropies on the formation and movement of domain walls.

Many of these questions are related to equally important technological problems. For example, the path of a domain wall across a magnetic substrate may be seen either as a challenge to the predictive power of theory or as a limitation on the maximum density of recording data on magnetic storage media. Also, the formation of magnetic domains in thin magnetic films or in fabricated structures with dimensions comparable to wall widths must be understood to produce the newest generation of tape or disk heads and nonvolatile memory systems.

All these issues can be summarized as the need to relate macroscopic magnetic properties to microscopic magnetic structure. What is required is a technique to image directly the vector magnetization of the surface of a ferromagnet. The way in which this can be realized can be seen from an experiment by Unguris and co-workers (*23*), in which unpolarized electrons were focused on a single domain of a ferromagnetic glass ($Fe_{81.5}B_{14.5}Si_4$) and the secondary

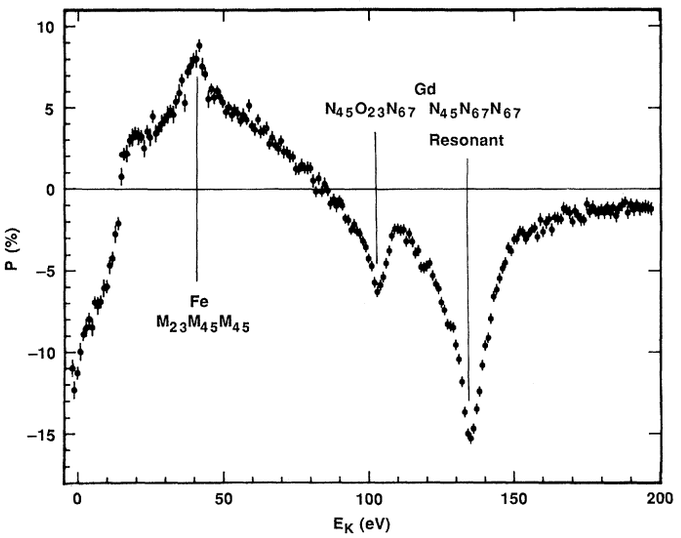

Fig. 3. The secondary electron spin polarization as a function of kinetic energy for a one-monolayer gadolinium film on an Fe(100) crystal surface. The primary energy was 2500 eV, and the measurement temperature was 150 K. Auger transitions originating in iron and gadolinium yield polarizations of opposite sign, indicating an antiferromagnetic coupling of the gadolinium layer to the iron. [From (*22*)]

electron spin polarization and intensity were measured as a function of secondary electron energy. The secondary electron energy distribution had a sharp peak at a few electron volts of energy, as expected. The secondary electrons were polarized up to energies of about 25 eV, with the polarization peaking in the first few volts to a value approximately twice the higher energy value. Other experiments (*24–26*) on ferromagnets showed similar behavior. In all cases the electron polarization was proportional to and oriented with the magnetization of the target. This experiment showed that the high-energy incident beam had scattered ferromagnetically ordered electrons out of the valence band and into vacuum continuum states without appreciably disturbing their spin orientation.

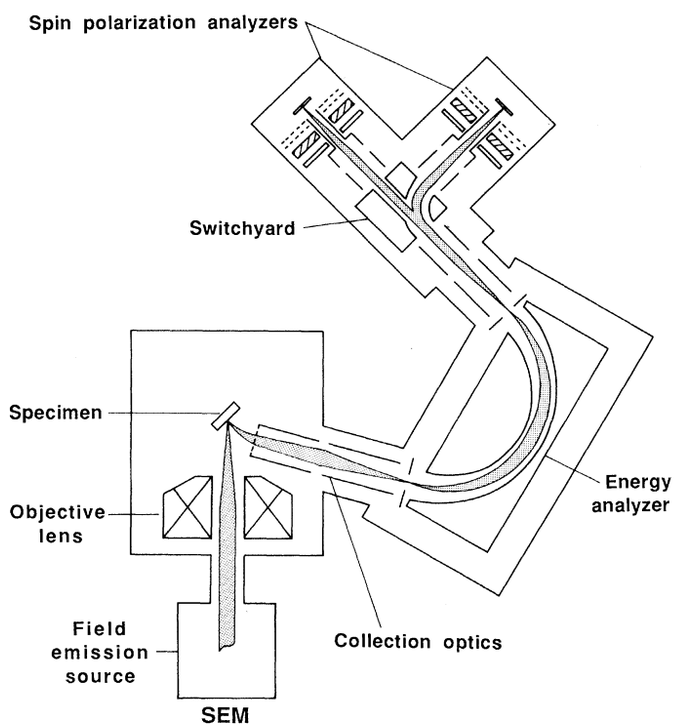

Fig. 4. A schematic view of the scanning electron microscope with two orthogonal spin analyzers to measure all three components of the electron spin polarization. The detectors and the optional energy analyzer are shown much larger than scale for clarity. [From (*27*)]

In scanning electron microscopy (SEM), images of surfaces are formed by rastering a highly focused electron beam across a sample, collecting the ejected secondary electrons, and intensifying a synchronized cathode-ray tube display in proportion to the number of secondaries collected. The experiment of Unguris and colleagues showed that, for the case of a ferromagnetic sample, these electrons have a spin polarization that reflects the local magnetic order just below the incident scanning beam. This information could be obtained by replacing the conventional secondary electron detector by one that measures both intensity and polarization. A high-efficiency, low-energy, compact detector (*6*) was designed for the purpose; a schematic diagram of a scanning electron microscope (*6, 27*) that has been modified by the addition of these detectors is shown in Fig. 4. After injection into the collection optics, the secondary electrons pass through an energy selector (which is optional in this application) and impinge on the gold surface of the polarization detector. Electrons are backscattered from the gold surface to opposite sides of the detector with different intensity if the incident beam has a polarization component normal to the scattering plane. With the use of a collection system consisting of channel plate electron multipliers and an anode divided into four quadrants, the detector can measure the two components of the electron beam polarization transverse to the beam direction. The third component of polarization is obtained by rotating the beam, but not the spin direction, in an electrostatic field to direct it to a second, orthogonal detector system. Scanning electron microscopy with polarization analysis (SEMPA) is capable of making ordinary SEM images of physical structure as well as images of the vector magnetization in three dimensions (*27, 28*) down to the resolution limit of the SEM, in this case 10 nm. (Compare this to optical domain imaging techniques, which have resolutions of approximately 1000 nm.) Further, in SEMPA the magnetic and intensity images are derived in fundamentally different ways, and hence they are independent. This is an important consideration because it allows the determination of which types of physical structure affect magnetic structure and which do not.

Because the polarization of the ejected electrons is analyzed, and because mean free path considerations permit only electrons from approximately the top 5 nm of sample to escape, the surface must be free of nonmagnetic contaminants. This is usually not practical in typical, high-vacuum electron microscopes. Therefore, an ultrahigh vacuum SEM or a scanning Auger microscope is used. Because SEMPA is sensitive to the topmost 5 nm of the target for its signal no loss in sensitivity is experienced when very thin magnetic films are analyzed.

Domains in cobalt, silicon-iron, and polycrystalline iron samples have been imaged (*29, 30*) with a scanning electron gun coupled with a high-energy Mott detection system. An example of a SEMPA image obtained (*6, 27*) with a scanning electron microscope with a field emission source, as illustrated in Fig. 4, is presented in Fig. 5. The domain pattern shown is from a silicon-iron crystal cut at a slight angle to the (100) direction. This image was chosen for its interesting domain structure even though the magnification was relatively low compared with that of images of submicrometer structures previously obtained (*6, 27*) with this instrument. The domains shown in Fig. 5B are typical of the closure domains that result as the bulk domains attempt to minimize the total magnetic

energy by forming additional domain structures at the surface boundary. The domain wall separating domains of opposing magnetization, seen in the lower left of the polarization image (Fig. 5B), has a jagged form to minimize the magnetic poles, which would otherwise be required and would contribute strongly to the total magnetic energy of the system. The structural defect at the center of Fig. 5A has a noticeable effect on the domain structure, but the other scratches are not important. The use of scanning AES would determine whether the defect corresponds to an anomalous composition or is simply structural.

Outlook

Because electron-based measurements are so widely used in surface studies, the advent of improved polarization sources and detectors has prompted a reexamination of spin-averaged electron spectroscopies and the new dimensions that polarization can add (*5, 32*). For example, in addition to the techniques discussed above, the deexcitation at a metal surface of metastable spin polarized He (2^3S) atoms provides a new way of studying surface magnetism (*32*).

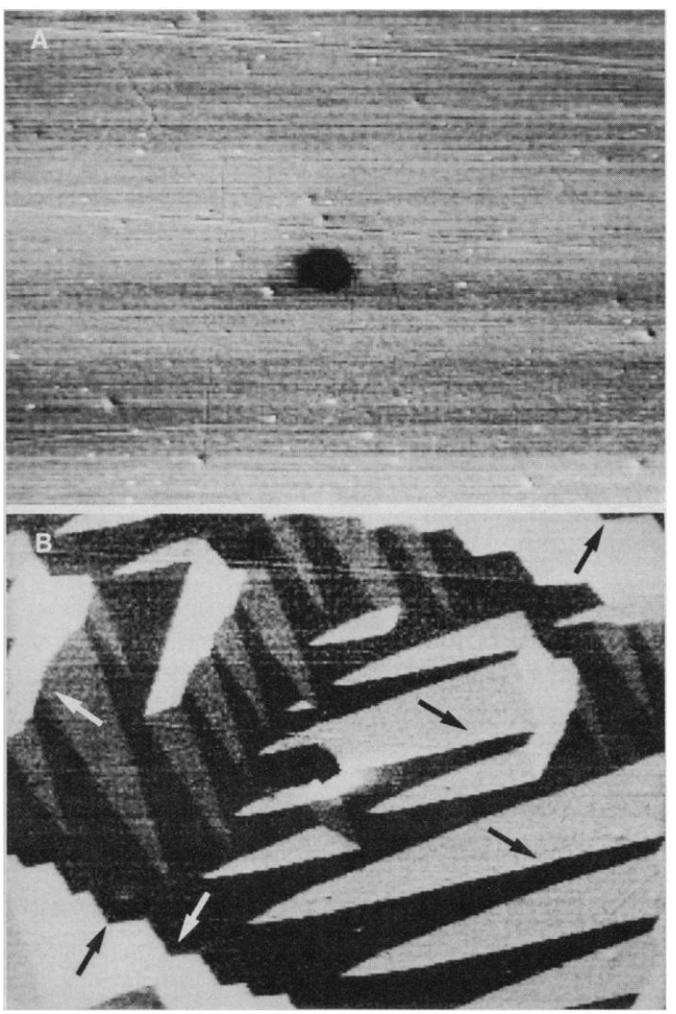

Fig. 5. (A) A conventional SEM micrograph of the surface of an Fe–3%Si crystal (x-axis length, 100 μm). (B) The simultaneously obtained map of the domain structure of the same region. There are four in-plane, easy axes of magnetization due to the cubic lattice anisotropy. The four gray levels indicate the four possible domain orientations, as indicated by the arrows. The domains are unaffected by most of the surface defects or scratches but are modified by the large defect at the center of the image.

Even spin-polarized photoemission, which has been an active field for some time now (*33*), will undoubtedly undergo significant changes as a result of the recent technical advances. New, compact, and efficient detectors should permit spin-polarized, angle-resolved photoemission experiments to be performed without the cumbersome apparatus of high-energy Mott detection. Further, the advent of undulator ports on major storage rings should compensate in photon flux for the loss in intensity mandated by polarization detectors that involve a scattering process. With these facilities, spin-resolved ultraviolet and x-ray photoemission experiments should be possible with a degree of complexity and a level of signal comparable to those of current spin-averaged experiments. The integration of compact spin analyzers with conventional Auger experiments could make spin-polarized AES a readily available surface analysis technique.

In addition to being stimulated by advances in experimental techniques, surface science will be spurred by the many advances in materials science. Systems can be fabricated to show the effects of reduced size or limited dimensionality. Multilayer structures are being grown epitaxially to thicknesses such that the resulting material has properties different from those of either constituent. Atomic engineering of new materials, which allow the investigation of new physical phenomena or form the basis of new devices, is an active area of research. Strains induced from a lattice mismatch can control the magnetic anisotropy and significantly modify magnetic properties. The collective effect of ferromagnetism depends strongly on nearest neighbor distance, and changes in the lattice near the interface can even affect the size of local moments. For example, recent advances in local-spin-density theory (*34*) have led to predictions that normally antiferromagnetic chromium will exist as a strong ferromagnet when grown as a monolayer on a gold (001) crystal surface or as part of a chromium-gold superstructure. The combination of the advances in theory, computation, polarization measurements, and molecular beam epitaxy is expected to nucleate an active field of investigation.

Because of the economic importance of magnetic technology, research directions will surely be influenced by technological needs. Many of the technological questions are also closely related to fundamental ones. The need for increased density of information storage demands smaller domain sizes and reduced dimensions in the magnetically active elements of devices such as disk heads. This requires a better understanding of domain formation and motion when the physical size of the structure becomes comparable to magnetic coherence lengths. A jagged domain wall can simultaneously be seen as an illustration of the interplay between terms in the system's Hamiltonian or as a source of noise in a transition-sensitive information storage system. Improvements in macroscopic properties such as coercivity may be brought about by a better understanding of the underlying microscopic physical structure. In new permanent magnet materials, exemplified by $Nd_2Fe_{14}B$, the role of defects, grain boundaries, and additional phases in the origin of the high coercivity remains to be understood. The SEMPA technique should find a great many applications in the study of the effects of size and dimensionality and in establishing the influence of microstructure on macroscopic properties.

Most of the experimental methods described here are still in their rudimentary stages, and some will undoubtedly be more useful than others. One thing is clear, however: now that spin-resolved electron beam measurements are practical and their value has been realized, studies of surface magnetism will rely heavily on this additional information channel.

REFERENCES AND NOTES

1. S. A. Goudsmit and G. E. Uhlenbeck, *Naturwissenschaften* **13**, 1953 (1925); *Nature (London)* **117**, 264 (1926).
2. J. Kessler, *Polarized Electrons* (Springer-Verlag, Berlin, 1976).
3. D. T. Pierce *et al.*, *Rev. Sci. Instrum.* **51**, 478 (1980).
4. D. T. Pierce and F. Meier, *Phys. Rev. B* **13**, 5484 (1976).
5. J. Kirschner, *Polarized Electrons at Surfaces* (Springer-Verlag, Berlin, 1985).
6. J. Unguris, D. T. Pierce, R. J. Celotta, *Rev. Sci. Instrum.* **57**, 1314 (1986).
7. J. Kirschner, *Phys. Rev. B* **30**, 415 (1984).
8. D. T. Pierce, R. J. Celotta, J. Unguris, H. C. Siegmann, *ibid.* **26**, 2566 (1982).
9. R. Feder and H. Pleyer, *Surf. Sci.* **117**, 285 (1982).
10. G. Rado, *Bull. Am. Phys. Soc. II* **2**, 127 (1957).
11. D. L. Mills and A. A. Maradudin, *J. Phys. Chem. Solids* **28**, 1855 (1967).
12. K. Binder and P. C. Hohenberg, *Phys. Rev. B* **6**, 3461 (1972).
13. S. F. Alvarado, M. Campagna, F. Cicacci, H. Hopster, *J. Appl. Phys.* **53**, 7920 (1982).
14. D. Weller, S. F. Alvarado, W. Gudat, K. Schroder, M. Campagna, *Phys. Rev. Lett.* **54**, 1555 (1985).
15. K. Binder and D. P. Landau, *ibid.* **52**, 318 (1984).
16. H. W. Diehl and A. Nüsser, in preparation.
17. E. Kisker, K. Schroder, M. Campagna, W. Gudat, *Phys. Rev. Lett.* **52**, 2285 (1984); *Phys. Rev. B* **31**, 329 (1985).
18. E. M. Haines, R. Clauberg, R. Feder, *Phys. Rev. Lett.* **54**, 932 (1985).
19. J. Unguris, A. Seiler, R. J. Celotta, D. T. Pierce, P. D. Johnson, N. V. Smith, *ibid.* **49**, 1047 (1982).
20. C. S. Feigerle, A. Seiler, J. L. Pena, R. J. Celotta, D. T. Pierce, *ibid.* **56**, 2207 (1986).
21. M. Landolt, in *Polarized Electrons in Surface Physics*, R. Feder, Ed. (World Scientific, Singapore, 1985), pp. 385–421.
22. M. Taborelli, R. Allenspach, G. Boffa, M. Landolt, *Phys. Rev. Lett.* **56**, 2869 (1986).
23. J. Unguris, D. T. Pierce, A. Galejs, R. J. Celotta, *ibid.* **49**, 72 (1982).
24. E. Kisker, W. Gudat, K. Schroder, *Solid State Commun.* **44**, 623 (1982).
25. H. Hopster *et al.*, *Phys. Rev. Lett.* **50**, 70 (1983).
26. M. Landolt, R. Allenspach, D. Mauri, *J. Appl. Phys.* **57**, 3626 (1985).
27. J. Unguris, G. G. Hembree, R. J. Celotta, D. T. Pierce, *J. Magn. Magnetic Mater.* **54–57**, 1629 (1986).
28. R. J. Celotta and D. T. Pierce, in *Microbeam Analysis*, K. F. J. Heinrich, Ed. (San Francisco Press, San Francisco, 1982), pp. 469–471.
29. K. Koike and K. Hayakawa, *J. Appl. Phys.* **57**, 4244 (1985).
30. K. Koike, H. Matsuyama, H. Todokoro, K. Hayakawa, *Jpn. J. Appl. Phys.* **24**, L542 (1985); *ibid.*, p. 1833.
31. R. Feder, Ed., *Polarized Electrons in Surface Physics* (World Scientific, Singapore, 1985).
32. M. Onellion, M. W. Hart, F. B. Dunning, G. K. Walters, *Phys. Rev. Lett.* **52**, 380 (1984).
33. H. C. Siegmann, F. Meier, M. Erbudak, M. Landolt, *Adv. Electron. Electron Phys.* **62**, 1 (1984).
34. C. L. Fu and A. J. Freeman, *Phys. Rev. B* **33**, 1755 (1986).

35. We are pleased to acknowledge our collaborators in the SEMPA measurements, J. Unguris and G. Hembree, for their contributions to the previously unpublished work shown in Fig. 5. Supported in part by the Office of Naval Research.

Corrosion of Electronic Materials and Devices

R. B. COMIZZOLI, R. P. FRANKENTHAL, P. C. MILNER, J. D. SINCLAIR

Electronic materials and devices corrode in the same ways as automobiles, bridges, and pipelines, but their typically small dimensions make them orders of magnitude more susceptible to corrosion failure. As elsewhere, the corrosion involves interactions with the environment. Under control, these interactions can be put to use, as in the formation of protective and functional oxide films for superconducting devices. Otherwise, they cause damage, as in the electrolytic dissolution of conductors, even gold, in the presence of humidity and ionic contamination from atmospheric particles and gases. Preventing corrosion entails identifying the damaging interactions and excluding species that allow them to occur.

ALMOST EVERY USE OF MATERIALS INVOLVES THE POSSIBILITY of corrosion. This arises from the thermodynamic instabilities inherent in the interactions between the materials and their use environments. The importance of corrosion to technology is reflected in a long history of work in corrosion science and engineering that incorporates knowledge from many scientific disciplines. Corrosion may occur uniformly or locally and at a continuous or discontinuous rate. It eventually results in material failure, and the time scale for this failure determines either the useful life of the structure of which the material is a part or the time cycle required for maintenance and repair. Corrosion and catastrophic corrosion failures are minimized by the selection of appropriate combinations of corrosion-resistant materials, such as protective coatings, and by the application of corrosion-preventing technologies, such as inhibitor systems.

The current advanced state of the electronics industry is based largely on the use of materials selected for their electronic, magnetic, or optical properties and not for their corrosion resistance. Continued advances depend on the use of new materials with improved and novel properties and on new combinations of materials in novel structures. The devices and other components utilizing these materials are typically incorporated in large numbers in electronic systems and must perform with a high degree of reliability if the systems are to function. Component failure rates corresponding to a few tens of failures in 10^9 operating hours (FIT's) are often necessary, even with redundant system designs. These levels of reliability are achievable only if failures from corrosion are essentially eliminated.

The corrosion phenomena encountered in electronic materials and devices are the same as those found in automobiles, bridges, pipelines, and other familiar objects in the everyday world. Like steel, both elemental and compound semiconductors, ranging from silicon to gallium arsenide to mercury cadmium telluride, are subject to atmospheric corrosion, as are most of the metals and alloys used in electronic devices and systems. As in plumbing and construction, combinations of dissimilar materials, such as aluminum alloys and gold or copper, may suffer from galvanic corrosion through the formation of local electrochemical cells. Finally, as in almost all

The authors are with AT&T Bell Laboratories, Murray Hill, NJ 07974.